Efficient Quantum Transduction Using Anti-Ferromagnetic Topological Insulators

Haowei Xu[1], Changhao Li[1,2], Guoqing Wang[1,2], Hao Tang[3],

Paola Cappellaro[1,2,4, †], and Ju Li[1,3, ‡]

[1] Department of Nuclear Science and Engineering, Massachusetts Institute of Technology, Cambridge, Massachusetts 02139, USA

[2] Research Laboratory of Electronics, Massachusetts Institute of Technology, Cambridge, MA 02139, USA

[3] Department of Materials Science and Engineering, Massachusetts Institute of Technology, Cambridge, Massachusetts 02139, USA

[4] Department of Physics, Massachusetts Institute of Technology, Cambridge, MA 02139, USA

* Corresponding authors: † pcappell@mit.edu, ‡ liju@mit.edu

Abstract

Transduction of quantum information between distinct quantum systems is an essential step in various applications, including quantum networks and quantum computing. However, mediating photons of vastly different frequencies and designing high-performance transducers are challenging, due to multifaceted and sometimes conflicting requirements. In this work, we first discuss some general principles for quantum transducer design, and then propose solid-state anti-ferromagnetic topological insulators to serve as highly effective transducers. First, topological insulators exhibit band-inversion, which can greatly enhance their optical responses. This property, coupled with robust spin-orbit coupling and high spin density, results in strong nonlinear interaction in magnetic topological insulators, thereby substantially improving transduction efficiency. Second, the anti-ferromagnetic order can minimize the detrimental influence on other neighboring quantum systems due to magnetic interactions. Using $MnBi_2Te_4$ as an example, we showcase that *single-photon* quantum transduction efficiency exceeding 80% can be achieved with modest experimental requirements, while the transduction bandwidth can reach the GHz range. The strong nonlinear photonic interactions in magnetic topological insulators can find diverse applications, including the generation of entanglement between photons of disparate frequencies and quantum squeezing.

Introduction. Quantum information processing systems typically operate in distinct frequency domains. For example, superconducting qubits, one of the leading platforms in quantum computation, work at microwave (MW) frequencies. Meanwhile, photons with infrared (IR) to visible frequencies can serve as flying qubits for long-distance communication. Therefore, efficient quantum transduction between different frequency domains is crucial to harness the advantages of different platforms in hybridized quantum systems and quantum networks.

We specifically focus on the transduction between MW and IR photons. An ideal quantum transducer should exhibit strong interaction with both MW and IR photons, so that high transduction efficiency and bandwidth can be enabled. Meanwhile, it is also necessary to minimize any adverse influence on the quantum system (e.g., superconducting qubits) resulting from the coupling with the transducer. Diverse transduction schemes have been explored, involving e.g., neutral atoms [1,2], rare-earth-doped crystals [3,4], optomechanical devices [5–7], electro-optics [6–8], and magnons [9,10]. Unfortunately, it is a nontrivial task to identify a high-performance transducer. For example, while Rydberg atoms have relatively strong interaction with MW photons, their large polarizabilities can also lead to decoherence and even destroy the superconducting states of superconducting qubits [11,12]. Electro-optical devices, on the other hand, suffer from weak nonlinearities typically below 10^3 pm/V [13].

Magnetic topological insulators (MTIs) [14–17] are a class of magnetic materials with nontrivial electronic band topology, which have attracted wide interest in condensed matter physics. In MTIs, the combination of the nontrivial electronic band topology and magnetism leads to a wealth of novel properties, such as the quantum anomalous Hall effect [16] and axion electrodynamics [17]. These unique properties suggest novel applications of MTIs. In this work, we propose that MTIs, particularly anti-ferromagnetic topological insulators (AFMTIs), hold great potential in quantum information science as well, thanks to their enhanced linear and nonlinear optical response. Specifically, we will demonstrate that AFMTI can serve as efficient quantum transducers, which could enable high transduction efficiency and wide bandwidth exceeding GHz even at *single-photon* level. Regarding transduction applications, the inherent collective spin excitation (magnon) frequencies in magnetic materials typically fall in the MW range [18–20]. Considering the ultra-large number density ($\sim 10^{28}$ m^{-3}) of magnetic moments, this suggests that magnetic materials can have strong coupling with MW photons [9,10]. Additionally, if anti-ferromagnetic (AFM) materials are used as the transducer, the influence on nearby quantum systems can be minimized,

because AFM materials have vanishing total magnetic moments. Indeed, these features have elicited great interest in AFM spintronics [18,19].

Moreover, the nontrivial electronic band topology of MTIs can greatly boost the quantum transduction performance. Topological insulators feature band inversion [21,22], whereby the energy ordering of normal valence and conduction bands is inverted in certain regions of the Brillouin zone. The band inversion usually leads to stronger hybridization between valence and conduction band wavefunctions, which in turn results in larger Berry curvature and stronger coupling with visible and IR photons [23–26]. Meanwhile, topological insulators typically possess heavy elements and thus strong spin-orbit coupling (SOC), which accelerates the conversion between spin and orbital dynamics and further improves the transduction efficiency in MTIs. Synergistically, these features contribute to the proposed performance of MTI quantum transducers.

In the following, we will first discuss some general principles to improve transduction efficiency. Then, we will introduce the mechanism of quantum transduction in magnetic materials and explain why AFMTIs can be efficient transducers. Using $MnBi_2Te_4$ [27–29] as an example, we will demonstrate the enhanced coupling strength with MW and IR photons in AFMTIs. We will show that quantum transduction using $MnBi_2Te_4$ as the transducer can achieve a single-photon transduction efficiency over 80% with modest experimental requirements. The bandwidth of the transduction can potentially reach GHz, nearly two orders of magnitude larger than the typical bandwidth based on other transduction schemes [30]. The intrinsic second-order $\chi^{(2)}$ nonlinearity of $MnBi_2Te_4$ can reach 10^6 pm/V, orders of magnitude larger than that of typical electro-optical materials [13] and topologically trivial magnetic materials [9,10]. Besides, the transduction scheme we proposed is applicable in centrosymmetric materials, in contrast to the electro-optical effect, which requires inversion symmetry breaking.

Design principles for efficient transducers. The purpose of the transduction process is to convert MW photons to IR photons (or vice versa), whose frequencies are ω_{MW} and ω_{IR}, respectively. A pumping laser with a frequency $\omega_{pump} = \omega_{IR} - \omega_{MW}$ is applied, so that energy conservation can be satisfied. To achieve efficient quantum transduction, the transducer should have strong coupling with both MW and IR photons, which have drastically different frequencies by 4-5 orders of magnitude. Establishing strong coupling between quantum degrees of freedom (DoF) generally

3

requires resonance (frequency matching) conditions. However, a single DoF cannot be resonant with two vastly different frequencies simultaneously. Actually, this leads to an intrinsic limit on the coupling strength of the electro-optical effect from pure electronic responses [31], whereby the MW and the IR/visible photons are both coupled to the electronic orbital transitions (~ 1 eV) in semiconductors. The MW photons (~ 0.1 meV) are far off-resonance, leading to weak responses. Indeed, in materials with soft phonon modes, such as $BaTiO_3$ [32,33], the major contribution to the electro-optical responses comes from ionic (i.e., phonon) responses [13], whereby the detuning between phonons and MW photons can be smaller.

A potentially better strategy is to employ a transducer with two DoFs designed to be (nearly) resonant with MW and IR photons, respectively. These two DoFs are then coupled by a specific internal interaction within the transducer. For example, using Rydberg atoms, the MW photons are coupled with the transitions between two highly excited Rydberg states. By judiciously selecting the principal quantum numbers of the Rydberg states, nearly resonant conditions can be satisfied, which can significantly improve the coupling strength. Unfortunately, this also leads to some detrimental effects, such as large polarizabilities [30].

Similarly, the transduction scheme based on rare-earth-ion doped crystals [3,4] or magnons [9,10] utilizes the two intrinsic DoFs of electrons, namely spin and orbital excitations, which are internally coupled by the spin-orbit coupling (SOC) ubiquitous in atoms, molecules, and solid-state systems. The orbital excitation energy of electrons is usually on the order of 1 eV, facilitating the coupling with photons in the visible or IR range. To utilize the spin DoF, it is necessary to have unpaired electron spins (magnetic moments), which can result from dopants, such as rare-earth-ions, in crystals. In terms of coupling strength, a more favorable option is to use pristine magnetic materials [9,10], where the number density of electron magnetic moments can reach 10^{28} m^{-3}. Besides, external magnetic fields are not necessary for sustaining the spin splitting in magnetic materials, which can be advantageous as well. In ferromagnetic materials, the spin excitation (magnon) frequency ω_m is typically on the order of GHz and is close to MW frequencies, but the macroscopic magnetic moments and the resultant magnetic fields can adversely affect the performance of the quantum objects (e.g., superconducting qubits) adjacent to the transducer [9,10].

In this regard, we suggest using AFM materials, whose net macroscopic magnetic moment is zero. However, a potential concern arises from the high magnon frequencies ω_m in AFM materials (up to the THz range [18,19]), which can lead to relatively large detuning from the frequencies of MW photons. Therefore, soft AFM materials with relatively low magnon frequencies (down to 100 GHz) would be more favorable. The detuning can also be reduced (potentially to zero in soft AFM materials) using magnetic fields. Furthermore, it is crucial to establish a general approach for selecting or designing AFM materials that can strongly interact with IR and/or MW photons, so that the overall transduction efficiency can be improved.

The discussions above lead us to the proposal of using AFMTIs as the transducer. As we will explain in more detail later, compared with topologically trivial AFM materials, AFMTIs have enhanced coupling strength with IR photons, thanks to their band inversion. AFMTIs also possess strong intrinsic SOC, resulting in rapid internal conversion between spin and orbital dynamics, which is beneficial for quantum transduction. Consequently, the transduction efficiency can be strong despite the relatively large frequency detuning between AFM magnons and MW photons. In the following, we will argue that AFMITs can serve as efficient quantum transducers, and their transduction performance can be orders of magnitude better than topologically trivial AFM materials such as Cr_2O_3.
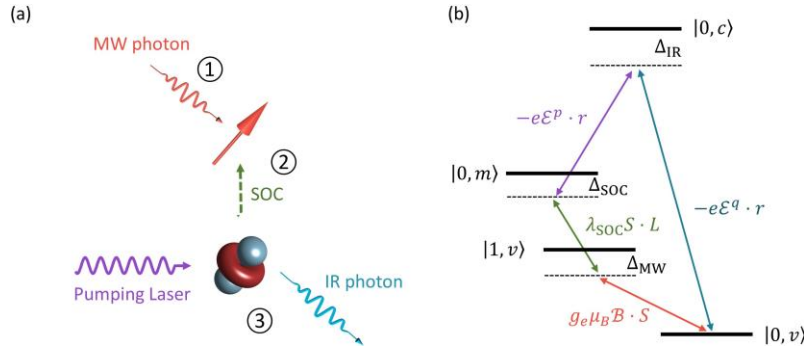
Figure 1. Schematic diagram showing the mechanism of the transduction based on MTIs (the MW→IR process). MW and IR photons interact with the spin and orbital degrees of freedom of the electrons, respectively, which are internally coupled by SOC. A pumping laser is applied so that energy conservation can be fulfilled. (b) Energy level diagram of the transduction process. See main text for description of scheme and labels.

Transduction mechanism in anti-ferromagnetic materials. We first examine the mechanism of transduction using AFM materials. Although magnons in AFM materials are collective spin excitations, for the sake of simplicity, we will treat every unit cell individually. This approach is valid since photons only interact with magnons with wavevectors $\boldsymbol{k} \approx 0$. SOC will only be considered for the interconversion between spin and orbital dynamics and will be disregarded elsewhere. The quantum state of electrons can be labeled with $|\mathcal{N}, m\rangle$, where the electron wavevector $\boldsymbol{k}$ is omitted, $\mathcal{N} = 0,1,2, \dots$ denotes the number of magnons, while m denotes the orbital state of the electrons. The energy of $|\mathcal{N}, m\rangle$ is labeled as $E_{|\mathcal{N},m\rangle}$. We assume the electron is initially on the $|0, v\rangle$ state with v a valence state. The electron, as the transducer, shall return to this initial state after the whole transduction is finished. Note that the localized magnetic moment in magnetic materials mostly comes from the electron spins, instead of orbital angular momenta [34]. We will thus use spin and magnetic moment interchangeably hereafter.

To facilitate further discussions, we separate the transduction process into three steps (Figure 1a). First, the magnetic field $\mathcal{B}$ of the MW photon interacts with the electron spin S through the Zeeman interaction $H_Z = g_e \mu_B S \cdot \mathcal{B}$, where g_e is the electron g-factor and μ_B is the Bohr magneton. Due to the Zeeman interaction, one magnon can be excited and the electron thus jumps to the $|1, v\rangle$ state. The strength of this first step can be obtained from perturbation theory, and can be characterized by $\xi_{MW} = \frac{\langle 0,v|H_Z|1,v\rangle}{\Delta_{MW}}$, where $\Delta_{MW} \equiv E_{|1,v\rangle} - E_{|0,v\rangle} - \omega_{MW} = \omega_m - \omega_{MW}$ is the frequency mismatch between the MW photon and the magnon. Note that in practice Δ_{MW} should be large enough to avoid the resonant absorption of the MW photon by magnons, which is undesirable for transduction.

Next, SOC induces a $|1, v\rangle \rightarrow |0, m\rangle$ transition, whereby the electron spin DoF returns to the ground state ($\mathcal{N} = 0$), while the orbital DoF transits from $|v\rangle$ to an intermediate state $|m\rangle$. The strength of this second step is characterized by $\xi_{SOC} = \frac{\langle 1,v|H_{SOC}|0,m\rangle}{\Delta_{SOC}}$, where $H_{SOC} = \lambda_{SOC} S \cdot L$ is the SOC Hamiltonian, λ_{SOC} is the SOC strength, L is the angular momentum operator, while $\Delta_{SOC} \equiv E_{|0,m\rangle} - E_{|1,v\rangle} - \omega_{MW}$ is the energy detuning. Here the SOC is considered a static interaction. Generally, the numerator $\langle 1, v|H_{SOC}|0, m\rangle$ has a similar order of magnitude for all possible m. Hence, ξ_{SOC} can be maximized when Δ_{SOC} is minimized. This condition is satisfied

when $m = v$, whereby one has $\Delta_{SOC} \sim 100$ GHz ~ 1 meV, corresponding to MW frequencies, otherwise one usually has $\Delta_{SOC} \sim 1$ eV for $m \neq v$.

During the third step of the transduction process, two IR fields p and q interact with the electron orbital motion via the electric dipole interaction $H_d^{p\,(q)} = -e\mathcal{E}^{p\,(q)} \cdot r$, where r is the electron position operator, and $\mathcal{E}^{p\,(q)}$ is the IR electric field. For definiteness, the p and q fields will hereafter correspond to the pumping laser and the transduced IR photon, respectively (Figure 1). Specifically, the $|0, m\rangle$ electron jumps to another intermediate state $|0, c\rangle$ via H_d^p, whereby a p-photon is absorbed, and then returns to the initial state $|0, v\rangle$ via H_d^q, whereby a q-photon is emitted. The strength of this two-photon process can be characterized by $\xi_{IR} = \sum_c \frac{\langle 0,m|H_d^p|0,c\rangle\langle 0,c|H_d^q|0,v\rangle}{\Delta_{IR}}$ with $\Delta_{IR} \equiv E_{|0,c\rangle} - E_{|0,v\rangle} - \omega_{IR}$, where ω_{IR} is the frequency of the q-photon. But to the leading order of the analysis, we can also take ω_{IR} to be the frequency of the p-photon due to the small frequency difference between the two IR fields.

Altogether, the MW to IR transduction process is: (1) incident MW photons (virtually) excite magnons (spin excitations); (2) the spin excitations are converted to orbital excitations through SOC; (3) following the laser-pumped transitions, the orbital excitations decay, resulting the emission of IR photons (Figure 1). In principle, these three steps have equal status and can occur simultaneously. The separation into three steps here should be regarded as artificial, which leads to the fact that ξ_{MW} and ξ_{SOC} are unitless, while ξ_{IR} has a unit of energy. A more rigorous treatment can be formulated using third-order perturbation theory [35]. The overall coupling strength of the transduction can be expressed as [see Supplementary Materials (SM) for details]

$$\mathcal{G} \approx \frac{N_s g_e \mu_B \mathcal{S}\,\mathcal{B} \cdot \lambda_{SOC} \cdot \varepsilon_0 \chi_r(\omega_{IR}) V_{cell} \mathcal{E}^p \mathcal{E}^q}{\Delta_{MW}\Delta_{SOC}} \tag{1}$$

Here N_s and V_{cell} are the total number of magnetic moments and the volume of the unit cell. In AFM materials, the magnetic moments are fully concentrated, and one has $N_s V_{cell} \sim V_0$ with V_0 the volume of the crystal. Meanwhile, ε_0 and $\chi_r(\omega_{IR})$ are the vacuum permittivity and the optical susceptibility of the host material, respectively. From Eq. (1), one can observe that the coupling strength $\mathcal{G}$ is determined by the product of the strength of the three steps, which are represented by $N_s g_e \mu_B \mathcal{S}\mathcal{B}$, λ_{SOC}, and $\varepsilon_0 \chi_r(\omega_{IR}) V_0 \mathcal{E}^p \mathcal{E}^q$, respectively. In addition, $\mathcal{G}$ is also influenced by Δ_{MW} and Δ_{SOC}. For AFM magnons, one typically has $\Delta_{MW\,(SOC)} \gtrsim 100$ GHz,

which is well above the magnon linewidth [18,19]. Δ_{MW} and Δ_{SOC} can potentially be reduced by applying externally static magnetic fields $\mathcal{B}_0$, which modulate magnon frequencies. Fortunately, $\mathcal{G}$ is sufficiently strong even if $\mathcal{B}_0 = 0$, as demonstrated later.

Additionally, we would like to remark that the transduction scheme described above can be used in centrosymmetric materials. Specifically, under spatial inversion operation, $\mathcal{G} \sim \mathcal{B}\mathcal{E}^2$ in Eq. (1) is invariant, as $\mathcal{B}$ and $\mathcal{E}$ get a $+1$ and -1 sign, respectively. In comparison, the electro-optical effect requires inversion symmetry breaking, because its coupling strength $\mathcal{G}_{EO} \sim \mathcal{E}^3$ undergoes a sign change under spatial inversion, hence it must be zero in centrosymmetric materials.

Enhanced coupling strength in material topological insulators. To improve the transduction performance, it is essential to enhance $\mathcal{G}$. This involves optimizing each of the three steps described above. Typically, the electron g-factor is close to 2 in magnetic materials [34,36–39]. Hence, to improve the strength of the first step (Zeeman interaction), one has to increase the number of electron spins N_s. This highlights the advantage of using magnetic materials, where the magnetic moments are fully concentrated [10], resulting in large N_s.

In contrast, the strengths of the second and third steps, which are determined by the SOC strength λ_{SOC} and the optical susceptibility $\chi_r(\omega_{IR})$, can vary significantly in different materials. Notably, λ_{SOC} and $\chi_r(\omega_{IR})$ in many scenarios are independent of each other. A strong SOC does not necessarily indicate strong optical responses, and vice versa [40]. Actually, some materials possessing strong optical responses, such as two-dimensional graphene [41] or MoS_2 [42], have weak SOC. Is there a systematic strategy to improve λ_{SOC} and $\chi_r(\omega_{IR})$ simultaneously? MTIs [14,15] provide a good solution. Strong SOC is usually a necessary condition for non-trivial electronic band topology, and thus topological insulators possess heavy elements and strong SOC [21,22]. Meanwhile, the electronic band inversion in topological insulators leads to significant wavefunction hybridization between the valence and conduction bands. This results in faster interband transition rates and thus stronger bulk optical responses [23–25], which has been verified experimentally [26].
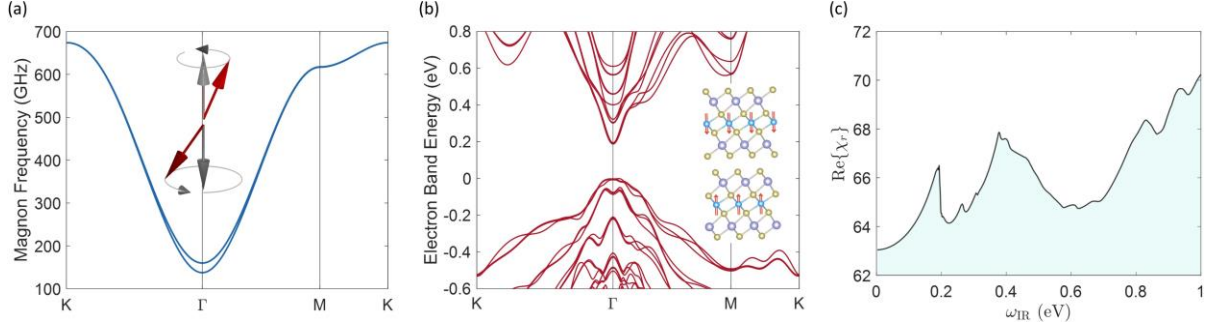
Figure 2. (a) Magnon dispersion of MnBi$_2$Te$_4$. Inset shows the spin precession in AFM materials when magnons are excited. Spins (red arrows) precess around the ground state (grey arrows, no magnons). (b) Electronic band structure of MnBi$_2$Te$_4$. Inset shows the atomic structure of MnBi$_2$Te$_4$. Blue: Mn; Purple: Bi; Brown: Te. The arrows on Mn atoms indicate the magnetic moments with AFM configuration. (c) The real part of the optical susceptibility of MnBi$_2$Te$_4$.

Next, we will use a well-known AFMTI MnBi$_2$Te$_4$ [27–29] as an example to demonstrate the potential of AFMTIs as quantum transducers. MnBi$_2$Te$_4$ has a layered structure (inset of Figure 2b), and on each layer, magnetic Mn atoms are sandwiched by Bi and Te atoms in the sequence of Te–Bi–Te–Mn–Te–Bi–Te. A minimal Hamiltonian for the local magnetic momentum ($S = 5/2$) of Mn atoms is [38,43]

$$\mathcal{H}_s = J_1 \sum_{\langle ij \rangle} \boldsymbol{S}_i \cdot \boldsymbol{S}_j + J_c \sum_{\langle ij \rangle'} \boldsymbol{S}_i \cdot \boldsymbol{S}_j + D_z \sum_i (S_i^z)^2 + \gamma_e \sum_i \boldsymbol{B} \cdot \boldsymbol{S}_i. \tag{2}$$

Here i, j label the Mn atoms, while $\langle ij \rangle$ and $\langle ij \rangle'$ indicate intra- and inter-layer nearest neighbors with spin-spin coupling strength $J_1 = -0.23 \text{ meV}$ and $J_c = 0.065 \text{ meV}$, respectively [38,43]. $D_z = -0.15 \text{ meV}$ characterizes the easy-axis magnetic anisotropy along z axis. With external magnetic field $\mathcal{B} = 0$, the intralayer exchange coupling between Mn atoms is ferromagnetic, while different layers are stacked with an AFM order. The magnon band structure obtained by linearizing Eq. (2) is shown in Figure 2a. The magnon frequency at the Γ-point is $\omega_m \approx 150 \text{ GHz}$, which is relatively low among AFM materials. This is advantageous compared with other hard AFM materials, since the detuning Δ_{MW} would be smaller for $\omega_{MW} \sim 10 \text{ GHz}$. Also, magnon relaxation due to e.g., magnon-magnon scatterings and magnon-photon scatterings can potentially be weaker [44,45] in soft magnetic materials such as MBT. This results from

smaller magnon-magnon coupling strength and smaller phase space of magnons/phonons in which the energy conservation law can be satisfied during the scattering process.

While Mn atoms provide magnetic moments, the heavy elements Bi and Te contribute to strong SOC in MnBi$_2$Te$_4$. According to our *ab initio* calculations, the SOC strength relevant to the transduction process is $\lambda_{SOC} \sim 47$ meV in MnBi$_2$Te$_4$ (see SM for details). As a comparison, the SOC strength in Cr$_2$O$_3$ [46], another prototypical AFM insulator, is only around 4 meV, as both Cr and O are light elements. This clearly demonstrates the advantage of using MnBi$_2$Te$_4$ for transduction. We will use $\lambda_{SOC} = 10$ meV for MnBi$_2$Te$_4$ in the following as a conservative estimation.

The strong SOC in MnBi$_2$Te$_4$ also leads to band inversion and nontrivial topology [27–29]. The electronic band structure of MnBi$_2$Te$_4$ is shown in Figure 2b. The inverted bandgap at the Γ point is around 0.2 eV, which falls in the mid-infrared range. The optical responses of MnBi$_2$Te$_4$ have been studied before [17,47–49]. Here we focus on the optical susceptibility $\chi_r(\omega_{IR})$, which can be expressed as

$$\chi_r(\omega_{IR}) = \frac{e^2}{\varepsilon_0} \int_k \frac{d\boldsymbol{k}}{(2\pi)^3} \sum_{c,v} \frac{|\langle 0,v|r|0,c\rangle|^2}{E_{|0,c\rangle} - E_{|0,v\rangle} - \omega_{IR}}, \tag{3}$$

where $\int d\boldsymbol{k}$ indicates the integration in the first Brillouin zone, while $c(v)$ indicates conduction (valence) bands. One can see that the magnitude of the numerator, $|\langle 0,v|r|0,c\rangle|^2$, strongly depends on the wavefunction overlap between valence and conduction bands, which is enhanced in topological materials because of the band inversion [23]. The calculated $\chi_r(\omega_{IR})$ of MnBi$_2$Te$_4$ is shown in Figure 3c, where one can see that $\chi_r(\omega_{IR} \to 0)$ is greater than 60, significantly larger than those of typical topologically trivial insulators. As an example, χ_r is below 15 in Cr$_2$O$_3$ for below bandgap frequencies (SM Figure S1). This corroborates the enhanced bulk optical responses in topological insulators [23–26].

To compared the coupling strength $\mathcal{G}$ with the ordinary definition of second-order susceptibility, we converting $\mathcal{B}$ to $\mathcal{E}$ using $\mathcal{B} = \mathcal{E}/c_0$ with c_0 the speed of light, yielding $\mathcal{G} = \chi_{eff}^{(2)} V_0 \varepsilon_0 \mathcal{E}^3$. Here the effective second-order susceptibility is $\chi_{eff}^{(2)} \gtrsim 10^6$ pm/V in MnBi$_2$Te$_4$ when $\Delta_{MW} = \Delta_{SOC} = 100$ GHz. As a comparison, in electro-optical materials, the second-order susceptibility is typically below 10^3 pm/V [13]. The large intrinsic nonlinearities also indicate

that MTIs can be efficient in other applications besides quantum transduction, such as two-mode squeezing [50] and entanglement generation [51,52].

Quantum transduction using MnBi₂Te₄ transducer. In the following, we will explore quantum transduction using MnBi₂Te₄ as the medium. The goal is to achieve efficient conversion between *single* MW and IR photons. Hence, we consider a setup where the MnBi₂Te₄ sample is coupled to both an IR cavity and an MW cavity. Additionally, a classical IR pumping laser with a frequency ω_{pump} is employed so that the frequency-matching condition ($\omega_{\text{MW}} + \omega_{\text{pump}} = \omega_{\text{IR}}$) can be satisfied. Accordingly, we second quantize the magnetic field $\mathcal{B}$ and electric field $\mathcal{E}^q$, and treat $\mathcal{E}^p$ as the classical pumping field in Eq. (1). To include the influence of magnon relaxation and dephasing, we (virtually) separate the transduction process into two stages, namely (i) MW photon to magnon and (ii) magnon to IR photon. Note that stage (ii) here combines steps 2 and 3 in Figure 1. The Hamiltonian in the rotating frame of the MW frequency can be expressed as,

$$\mathcal{H} = \delta_m a_m^\dagger a_m + \delta_{\text{IR}} a_{\text{IR}}^\dagger a_{\text{IR}} + \left(\mathcal{G}_{\text{MW}} a_{\text{MW}}^\dagger a_m + \mathcal{G}_{\text{IR}} a_{\text{IR}}^\dagger a_m + h.c. \right) \tag{4}$$

Here a_m, a_{IR}, and a_{MW} are the annihilation operators of magnon, IR photon, and MW photon, with $a^\dagger$ the corresponding creation operator. $h.c.$ stands for Hermitian conjugate. The first term in Eq. (4) is the detuning of the magnon frequency from the MW frequency, which can be tuned from around 100 GHz to 0 using a magnetic field up to 2 Tesla [38,39]. The second term is the detuning of the IR photon from perfect frequency matching condition ($\delta_{\text{IR}} \equiv \omega_{\text{IR}} - \omega_{\text{MW}} - \omega_{\text{pump}}$). A large transduction bandwidth indicates that the transduction efficiency remains high even if δ_{IR} is large. The third term in Eq. (4) corresponds to the conversion between IR/MW photons and magnons, and one can see that magnons serve as the medium between IR and MW photons. The collective coupling strengths are

$$\mathcal{G}_{\text{MW}} = \sqrt{N_s} g_e \mu_B S \, \mathcal{B}_{\text{MW}}^{\text{zpf}}$$

$$\mathcal{G}_{\text{IR}} = \sqrt{N_s} \frac{\lambda_{\text{SOC}} \cdot \varepsilon_0 \chi_r(\omega_{\text{IR}}) V_{\text{cell}} \mathcal{E}_{\text{IR}}^{\text{zpf}} \mathcal{E}_{\text{pump}}}{\Delta_{\text{SOC}}} \tag{5}$$

Here $\mathcal{E}_{\text{pump}}$ is the pumping field, while $\mathcal{B}_{\text{MW}}^{\text{zpf}} \equiv \sqrt{\frac{\mu_0 \omega_{\text{MW}}}{2V_{\text{MW}}}}$ and $\mathcal{E}_{\text{IR}}^{\text{zpf}} \equiv \sqrt{\frac{\omega_{\text{IR}}}{2\varepsilon_0(\chi_r+1)V_{\text{IR}}}}$ are the zero-point magnetic and electric fields of the MW and IR cavities, respectively. V_{MW} and V_{IR} are the mode volumes of the cavities. We assume that the MnBi₂Te₄ sample fills the IR cavity with mode

a mode volume of $V_{IR} = V_0 = 0.1 \text{ mm}^3$. Meanwhile, the mode volume of the MW cavity is $V_{MW} = 1 \text{ mm}^3$. We also take $\omega_{MW} = 10 \text{ GHz}$, $\omega_{IR} = 0.1 \text{ eV}$, and $\Delta_{SOC} = 100 \text{ GHz}$. This yields $\mathcal{G}_{MW} \approx 3 \text{ GHz}$ and $\mathcal{G}_{IR}[\text{GHz}] \approx 1.0 \times \mathcal{E}_{pump}[\text{kV} \cdot \text{m}^{-1}]$. In the following, we will take $\mathcal{E}_{pump} = 10 \text{ kV} \cdot \text{m}^{-1}$.

Note that one has $\mathcal{G} = \frac{\mathcal{G}_{MW}\mathcal{G}_{IR}}{\Delta_{MW}}$, where $\mathcal{G}$ is the overall coupling strength defined in Eq. (1). It should be emphasized that here we are considering the extreme case of *single-photon* quantum transduction, i.e., one MW photon to one IR photon, or the reverse, so $\mathcal{B}$ and $\mathcal{E}^q$ in Eq. (1) are replaced with zero-point cavity fields $\mathcal{B}_{MW}^{zpf}$ and $\mathcal{E}_{IR}^{zpf}$ in Eq. (5). If there are multiple MW or IR photons to be converted simultaneously [53,54], then the coupling strength can be enhanced by a factor of $\sqrt{N_{ph}}$ with N_{ph} the number of MW or IR photons in the cavities. This will improve the transduction performance.
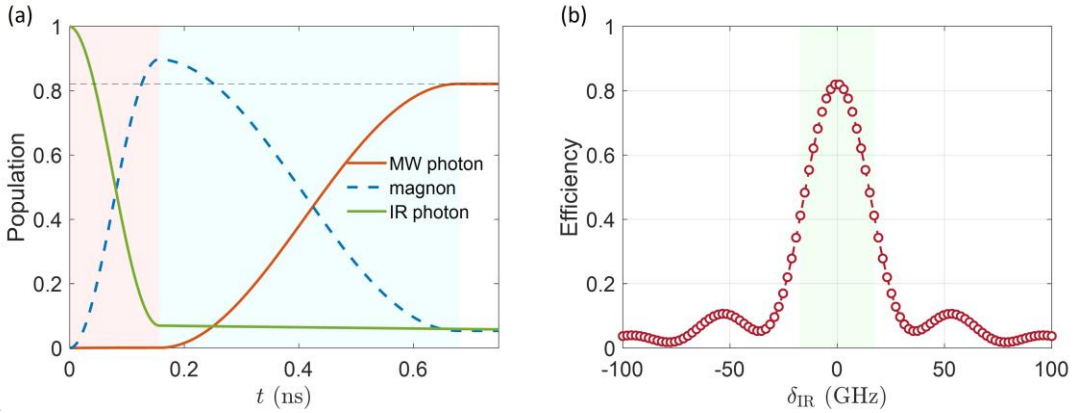
Figure 3. (a) Time evolution of the populations of MW photon, IR photon and magnon. Initially there is a single IR photon. Two SWAP gates are used for the transduction. The IR-magnon (MW-magnon) interaction is turned on in the pink (cyan) region. A single-photon transduction efficiency of 82% is reached (dashed horizontal line). (b) Single-photon transduction efficiency as a function of δ_{IR}. The green shaded area corresponds to the full width at half maximum. The parameters used in the simulations are described in the main text.

To evaluate the single-photon transduction efficiency, we adopt the quantum master equation

$$\frac{d\rho}{dt} = -i[\mathcal{H}, \rho] + \sum_o \kappa_o \zeta(o), \tag{6}$$

where ρ is the density matrix of the total system, $\zeta(o) \equiv o\rho o^\dagger - \frac{1}{2}o^\dagger o\rho - \frac{1}{2}\rho o^\dagger o$ is the Lindblad operator for a given operator o. Here we consider both the relaxation ($o = a_X$) and dephasing ($o = a_X^\dagger a_X$) processes ($X = m$, IR, and MW). The relaxation rates of magnons, IR photons and MW photons are estimated in the SM, where we consider multiple sources of noises, including defects and two-photon absorption processes. We will take the relaxation rate as $\kappa_{IR} = 0.3$ GHz , $\kappa_m = 0.1$ GHz , and $\kappa_{MW} = 10^{-3}$ GHz . Meanwhile, the dephasing rates are approximately taken as ten times the corresponding relaxation rate.

When the magnon detuning is $\delta_m = 0$ (on resonance with the MW photon), one can use two SWAP gates for efficient MW-IR transduction [55]. We will use IR to MW transduction as an example, while the reverse MW to IR transduction can be realized similarly. Firstly, the IR-magnon interaction is turned on for a certain amount of time that corresponds to a π-pulse. The population would be transferred from IR photon to magnon. Then, the IR-magnon interaction is turned off by detuning the IR cavity or tuning off the pumping laser, while the MW-magnon interaction is turned on for another π-pulse. The population would thus be transferred to MW photons. The time evolution of the populations is depicted in Figure 3(a), where one can see that a transduction efficiency of $\eta \approx 82\ \%$ can be realized by such a simple SWAP protocol. Note that η can be further enhanced by using a stronger $\mathcal{E}_{pump}$ (SM). The transduction bandwidth can be obtained by calculating the transduction efficiency η as a function δ_{IR}. As shown in Figure 3(b), the full width at half maximum (FWHM) bandwidth can exceed 10 GHz under the current setting.

The key to simultaneously improving the transduction efficiency and FWHM bandwidth is to have large coupling strength in Eq. (5). Hence, it is highly desirable to use materials with large intrinsic nonlinearities, whereby the coupling strength can be large enough under mild pumping fields. As discussed before, the nonlinearities of topologically trivial magnetic materials such as Cr_2O_3 or conventional electro-optical materials are usually two to three orders of magnitude lower than that of MBT. This indicates that if the same pumping laser with $\mathcal{E}_{pump} = 10\ kV \cdot m^{-1}$ is used, then the coupling strength would be much smaller, leading to extremely low transduction efficiency (below 1%). Conversely, to achieve the same transduction performance, then $\mathcal{E}_{pump}$ must be $10^2 \sim 10^3$ times stronger in Cr_2O_3 or conventional electro-optical materials. This could cause significant heating, photon relaxation, and damage in the materials, which can be catastrophic for the transduction process. As an example, the heating from defect states and two-photon absorption

scale as $\mathcal{E}_{\text{pump}}^2$ and $\mathcal{E}_{\text{pump}}^4$, respectively, so the temperature rise can reach hundreds of Kelvins when $\mathcal{E}_{\text{pump}}$ is increased to $10\,\text{MV} \cdot \text{m}^{-1}$ (SM). This again highlights the advantages of using MBT as the transducer, which enjoys exceptionally high intrinsic nonlinearities.

Until now, we considered quantum transduction to exemplify the potential of MTIs in quantum engineering. More broadly, MTIs can be advantageous in many other applications that require strong linear or nonlinear optical responses, such as quantum squeezing [50], entanglement generation [51,52], spontaneous parametric down-conversion [56], etc. Furthermore, $MnBi_2Te_4$ can be thinned down to single or multiple layers [27], leading to the possibility of quantum applications that extend to the two-dimensional limit [57].

In conclusion, we proposed that MTIs such as $MnBi_2Te_4$ can serve as efficient quantum transducers, thanks to their strong intrinsic optical nonlinearities. This is primarily due to topologically enhanced optical responses, robust spin-orbit coupling, together with high spin density in MTIs. We demonstrate that single-photon transduction efficiency over 80% and transduction bandwidth over GHz can be simultaneously achieved with modest experimental requirements, which can facilitate diverse applications in quantum information science and other fields.

Acknowledgment

References

[1]   J. Verdú, H. Zoubi, C. Koller, J. Majer, H. Ritsch, and J. Schmiedmayer, *Strong Magnetic Coupling of an Ultracold Gas to a Superconducting Waveguide Cavity*, Phys. Rev. Lett. **103**, 043603 (2009).
[2]   M. Hafezi, Z. Kim, S. L. Rolston, L. A. Orozco, B. L. Lev, and J. M. Taylor, *Atomic Interface between Microwave and Optical Photons*, Phys. Rev. A - At. Mol. Opt. Phys. **85**, 020302 (2012).
[3]   L. A. Williamson, Y.-H. Chen, and J. J. Longdell, *Magneto-Optic Modulator with Unit Quantum Efficiency*, Phys. Rev. Lett. **113**, 203601 (2014).
[4]   C. O'Brien, N. Lauk, S. Blum, G. Morigi, M. Fleischhauer, C. O'Brien, N. Lauk, S. Blum, G. Morigi, M. Fleischhauer, C. O'Brien, N. Lauk, S. Blum, G. Morigi, and M. Fleischhauer, *Interfacing Superconducting Qubits and Telecom Photons via a Rare-Earth-Doped Crystal*, Phys. Rev. Lett. **113**, 63603 (2014).
[5]   M. Aspelmeyer, T. J. Kippenberg, and F. Marquardt, *Cavity Optomechanics*, Rev. Mod. Phys. **86**, 1391 (2014).

[6]   R. W. Andrews, R. W. Peterson, T. P. Purdy, K. Cicak, R. W. Simmonds, C. A. Regal, and K. W. Lehnert, *Bidirectional and Efficient Conversion between Microwave and Optical Light*, Nat. Phys. 2014 104 **10**, 321 (2014).

[7]   T. Bagci, A. Simonsen, S. Schmid, L. G. Villanueva, E. Zeuthen, J. Appel, J. M. Taylor, A. Sørensen, K. Usami, A. Schliesser, and E. S. Polzik, *Optical Detection of Radio Waves through a Nanomechanical Transducer*, Nat. 2014 5077490 **507**, 81 (2014).

[8]   M. Tsang, *Cavity Quantum Electro-Optics*, Phys. Rev. A - At. Mol. Opt. Phys. **81**, 063837 (2010).

[9]   R. Hisatomi, A. Osada, Y. Tabuchi, T. Ishikawa, A. Noguchi, R. Yamazaki, K. Usami, and Y. Nakamura, *Bidirectional Conversion between Microwave and Light via Ferromagnetic Magnons*, Phys. Rev. B **93**, 174427 (2016).

[10]   J. R. Everts, M. C. Berrington, R. L. Ahlefeldt, and J. J. Longdell, *Microwave to Optical Photon Conversion via Fully Concentrated Rare-Earth-Ion Crystals*, Phys. Rev. A **99**, 063830 (2019).

[11]   M. H. Devoret and R. J. Schoelkopf, *Superconducting Circuits for Quantum Information: An Outlook*, Science (80-.). **339**, 1169 (2013).

[12]   M. Saffman, T. G. Walker, and K. Mølmer, *Quantum Information with Rydberg Atoms*, Rev. Mod. Phys. **82**, 2313 (2010).

[13]   A. K. Hamze, M. Reynaud, J. Geler-Kremer, and A. A. Demkov, *Design Rules for Strong Electro-Optic Materials*, Npj Comput. Mater. 2020 61 **6**, 1 (2020).

[14]   Y. Xu, L. Elcoro, Z. Da Song, B. J. Wieder, M. G. Vergniory, N. Regnault, Y. Chen, C. Felser, and B. A. Bernevig, *High-Throughput Calculations of Magnetic Topological Materials*, Nat. 2020 5867831 **586**, 702 (2020).

[15]   L. Elcoro, B. J. Wieder, Z. Song, Y. Xu, B. Bradlyn, and B. A. Bernevig, *Magnetic Topological Quantum Chemistry*, Nat. Commun. 2021 121 **12**, 1 (2021).

[16]   Y. Deng, Y. Yu, M. Z. Shi, Z. Guo, Z. Xu, J. Wang, X. H. Chen, and Y. Zhang, *Quantum Anomalous Hall Effect in Intrinsic Magnetic Topological Insulator MnBi2Te4*, Science (80-.). **367**, 895 (2020).

[17]   J. X. Qiu, C. Tzschaschel, J. Ahn, A. Gao, H. Li, X. Y. Zhang, B. Ghosh, C. Hu, Y. X. Wang, Y. F. Liu, D. Bérubé, T. Dinh, Z. Gong, S. W. Lien, S. C. Ho, B. Singh, K. Watanabe, T. Taniguchi, D. C. Bell, H. Z. Lu, A. Bansil, H. Lin, T. R. Chang, B. B. Zhou, Q. Ma, A. Vishwanath, N. Ni, and S. Y. Xu, *Axion Optical Induction of Antiferromagnetic Order*, Nat. Mater. 2023 225 **22**, 583 (2023).

[18]   P. Němec, M. Fiebig, T. Kampfrath, and A. V. Kimel, *Antiferromagnetic Opto-Spintronics*, Nature Physics.

[19]   J. Han, R. Cheng, L. Liu, H. Ohno, and S. Fukami, *Coherent Antiferromagnetic Spintronics*, Nat. Mater. 2023 1 (2023).

[20]   P. Pirro, V. I. Vasyuchka, A. A. Serga, and B. Hillebrands, *Advances in Coherent Magnonics*, Nat. Rev. Mater. 2021 612 **6**, 1114 (2021).

[21]   X. L. Qi and S. C. Zhang, *Topological Insulators and Superconductors*, Rev. Mod. Phys. **83**, 1057 (2011).

[22]   M. Z. Hasan and C. L. Kane, *Colloquium: Topological Insulators*, Rev. Mod. Phys. **82**, 3045 (2010).

[23]   H. Xu, J. Zhou, H. Wang, and J. Li, *Giant Photonic Response of Mexican-Hat Topological Semiconductors for Mid-Infrared to Terahertz Applications*, J. Phys. Chem. Lett. **11**, 6119 (2020).

[24]   H. Xu, H. Wang, J. Zhou, Y. Guo, J. Kong, and J. Li, *Colossal Switchable Photocurrents in Topological Janus Transition Metal Dichalcogenides*, Npj Comput. Mater. **7**, 31 (2021).

[25]   L. Z. Tan and A. M. Rappe, *Enhancement of the Bulk Photovoltaic Effect in Topological Insulators*, Phys. Rev. Lett. **116**, 237402 (2016).

[26]   J. Shi, H. Xu, C. Heide, C. HuangFu, C. Xia, F. de Quesada, H. Shen, T. Zhang, L. Yu, A. Johnson, F. Liu, E. Shi, L. Jiao, T. Heinz, S. Ghimire, J. Li, J. Kong, Y. Guo, and A. M. Lindenberg, *Giant Room-Temperature Nonlinearities in a Monolayer Janus Topological Semiconductor*, Nat. Commun. **14**, 4953 (2023).

[27]   J. Li, Y. Li, S. Du, Z. Wang, B. L. Gu, S. C. Zhang, K. He, W. Duan, and Y. Xu, *Intrinsic Magnetic Topological Insulators in van Der Waals Layered MnBi2Te4-Family Materials*, Sci. Adv. **5**, eaaw5685 (2019).

[28]   D. Zhang, M. Shi, T. Zhu, D. Xing, H. Zhang, and J. Wang, *Topological Axion States in the Magnetic Insulator MnBi2Te4 with the Quantized Magnetoelectric Effect*, Phys. Rev. Lett. **122**, 206401 (2019).

[29]   M. M. Otrokov, I. I. Klimovskikh, H. Bentmann, D. Estyunin, A. Zeugner, Z. S. Aliev, S. Gaß, A. U. B. Wolter, A. V. Koroleva, A. M. Shikin, M. Blanco-Rey, M. Hoffmann, I. P. Rusinov, A. Y. Vyazovskaya, S. V. Eremeev, Y. M. Koroteev, V. M. Kuznetsov, F. Freyse, J. Sánchez-Barriga, I. R. Amiraslanov, M. B. Babanly, N. T. Mamedov, N. A. Abdullayev, V. N. Zverev, A. Alfonsov, V. Kataev, B. Büchner, E. F. Schwier, S. Kumar, A. Kimura, L. Petaccia, G. Di Santo, R. C. Vidal, S. Schatz, K. Kißner, M. Ünzelmann,

C. H. Min, S. Moser, T. R. F. Peixoto, F. Reinert, A. Ernst, P. M. Echenique, A. Isaeva, and E. V. Chulkov, *Prediction and Observation of an Antiferromagnetic Topological Insulator*, Nature **576**, 416 (2019).

[30] K. Svensson, J. Lundqvist, E. Campos, al -, S. Forouzanfar, R. Mansour, E. Abdel-Rahman, N. Lauk, N. Sinclair, S. Barzanjeh, J. P. Covey, M. Saffman, M. Spiropulu, and C. Simon, *Perspectives on Quantum Transduction*, Quantum Sci. Technol. **5**, 020501 (2020).

[31] J. Sipe and A. Shkrebtii, *Second-Order Optical Response in Semiconductors*, Phys. Rev. B **61**, 5337 (2000).

[32] M. Zgonik, P. Bernasconi, M. Duelli, R. Schlesser, P. Günter, M. H. Garrett, D. Rytz, Y. Zhu, and X. Wu, *Dielectric, Elastic, Piezoelectric, Electro-Optic, and Elasto-Optic Tensors of $BaTiO_3$ Crystals*, Phys. Rev. B **50**, 5941 (1994).

[33] K. D. Fredrickson, V. V. Vogler-Neuling, K. J. Kormondy, D. Caimi, F. Eltes, M. Sousa, J. Fompeyrine, S. Abel, and A. A. Demkov, *Strain Enhancement of the Electro-Optical Response in BaTi O3 Films Integrated on Si(001)*, Phys. Rev. B **98**, 075136 (2018).

[34] M. S. Dresselhaus, *SOLID STATE PHYSICS PART III Magnetic Properties of Solids* (n.d.).

[35] H. Xu, H. Wang, and J. Li, *Abnormal Nonlinear Optical Responses on the Surface of Topological Materials*, Npj Comput. Mater. **8**, 111 (2022).

[36] G. G. Scott, *Review of Gyromagnetic Ratio Experiments*, Rev. Mod. Phys. **34**, 102 (1962).

[37] Y. Ogata, H. Chudo, M. Ono, K. Harii, M. Matsuo, S. Maekawa, and E. Saitoh, *Gyroscopic g Factor of Rare Earth Metals*, Appl. Phys. Lett. **110**, (2017).

[38] D. Lujan, J. Choe, M. Rodriguez-Vega, Z. Ye, A. Leonardo, T. N. Nunley, L. J. Chang, S. F. Lee, J. Yan, G. A. Fiete, R. He, and X. Li, *Magnons and Magnetic Fluctuations in Atomically Thin MnBi2Te4*, Nat. Commun. 2022 131 **13**, 1 (2022).

[39] S. M. Rezende, A. Azevedo, and R. L. Rodriguez-Suarez, *Introduction to Antiferromagnetic Magnons*, J. Appl. Phys. **126**, 151101 (2019).

[40] H. Xu, H. Wang, J. Zhou, and J. Li, *Pure Spin Photocurrent in Non-Centrosymmetric Crystals: Bulk Spin Photovoltaic Effect*, Nat. Commun. **12**, 4330 (2021).

[41] K. Batrakov, P. Kuzhir, S. Maksimenko, N. Volynets, S. Voronovich, A. Paddubskaya, G. Valusis, T. Kaplas, Y. Svirko, and P. Lambin, *Enhanced Microwave-to-Terahertz Absorption in Graphene*, Appl. Phys. Lett. **108**, 123101 (2016).

[42] L. M. Malard, T. V. Alencar, A. P. M. Barboza, K. F. Mak, and A. M. De Paula, *Observation of Intense Second Harmonic Generation from MoS2 Atomic Crystals*, Phys. Rev. B - Condens. Matter Mater. Phys. **87**, 201401 (2013).

[43] B. Li, D. M. Pajerowski, S. X. M. Riberolles, L. Ke, J. Q. Yan, and R. J. McQueeney, *Quasi-Two-Dimensional Ferromagnetism and Anisotropic Interlayer Couplings in the Magnetic Topological Insulator MnBi2Te4*, Phys. Rev. B **104**, L220402 (2021).

[44] S. M. Rezende and R. M. White, *Spin-Wave Lifetimes in Antiferromagnetic RbMnF3*, Phys. Rev. B **18**, 2346 (1978).

[45] T. Feng, L. Lindsay, and X. Ruan, *Four-Phonon Scattering Significantly Reduces Intrinsic Thermal Conductivity of Solids*, Phys. Rev. B **96**, 161201 (2017).

[46] L. M. Corliss, J. M. Hastings, R. Nathans, and G. Shirane, *Magnetic Structure of Cr2O3*, J. Appl. Phys. **36**, 1099 (1965).

[47] R. Fei, W. Song, and L. Yang, *Giant Linearly-Polarized Photogalvanic Effect and Second Harmonic Generation in Two-Dimensional Axion Insulators*, (2020).

[48] H. Wang and X. Qian, *Electrically and Magnetically Switchable Nonlinear Photocurrent in PT-Symmetric Magnetic Topological Quantum Materials*, Npj Comput. Mater. 2020 61 **6**, 1 (2020).

[49] Q. Ma, R. Krishna Kumar, S. Y. Xu, F. H. L. Koppens, and J. C. W. Song, *Photocurrent as a Multiphysics Diagnostic of Quantum Materials*, Nat. Rev. Phys. 2023 53 **5**, 170 (2023).

[50] A. I. Lvovsky, *Squeezed Light*, Photonics Sci. Found. Technol. Appl. **1**, 121 (2015).

[51] R. Sahu, L. Qiu, W. Hease, G. Arnold, Y. Minoguchi, P. Rabl, and J. M. Fink, *Entangling Microwaves with Light*, Science (80-.). **380**, 718 (2023).

[52] H. Y. Yuan, P. Yan, S. Zheng, Q. Y. He, K. Xia, and M. H. Yung, *Steady Bell State Generation via Magnon-Photon Coupling*, Phys. Rev. Lett. **124**, 053602 (2020).

[53]   A. P. Higginbotham, P. S. Burns, M. D. Urmey, R. W. Peterson, N. S. Kampel, B. M. Brubaker, G. Smith, K. W. Lehnert, and C. A. Regal, *Harnessing Electro-Optic Correlations in an Efficient Mechanical Converter*, Nat. Phys. **14**, 1038 (2018).

[54]   H. T. Tu, K. Y. Liao, Z. X. Zhang, X. H. Liu, S. Y. Zheng, S. Z. Yang, X. D. Zhang, H. Yan, and S. L. Zhu, *High-Efficiency Coherent Microwave-to-Optics Conversion via off-Resonant Scattering*, Nat. Photonics 2022 164 **16**, 291 (2022).

[55]   H. Xu, C. Li, G. Wang, H. Wang, H. Tang, A. R. Barr, P. Cappellaro, and J. Li, *Two-Photon Interface of Nuclear Spins Based on the Optonuclear Quadrupolar Effect*, Phys. Rev. X **13**, 011017 (2023).

[56]   C. Couteau, *Spontaneous Parametric Down-Conversion*, Https://Doi.Org/10.1080/00107514.2018.1488463 **59**, 291 (2018).

[57]   Q. Guo, X. Z. Qi, L. Zhang, M. Gao, S. Hu, W. Zhou, W. Zang, X. Zhao, J. Wang, B. Yan, M. Xu, Y. K. Wu, G. Eda, Z. Xiao, S. A. Yang, H. Gou, Y. P. Feng, G. C. Guo, W. Zhou, X. F. Ren, C. W. Qiu, S. J. Pennycook, and A. T. S. Wee, *Ultrathin Quantum Light Source with van Der Waals NbOCl2 Crystal*, Nat. 2023 6137942 **613**, 53 (2023).